Fully coupled discrete energy-averaged model for Terfenol-D

S. Chakrabarti[a)] and M. J. Dapino[b)]
Department of Mechanical and Aerospace Engineering, The Ohio State University, Columbus, Ohio 43210, USA

(Received 18 October 2011; accepted 12 January 2012; published online 6 March 2012)

A fully coupled 3D energy-avaraged model is presented which describes the magnetomechanical behavior of Terfenol-D. Conventional energy averaging with eight easy axis orientations yields an unphysical kink in the magnetization response and fails to describe the gradual approach to saturation present in Terfenol-D magnetostriction. Superposition of an empirically weighted global anisotropy energy onto an anisotropy energy locally defined around each easy axis eliminates the unphysical kink in the response, while an implicit definition of the domain volume fraction describes the gradual approach to saturation. Anhysteretic bulk material response is described through a weighted sum of individual domains; the weights (or domain volume fractions) are calculated using Boltzmann-type energy averaging. A hysteretic extension is built from an evolution equation for the domain volume fractions. Although solution of the implicit equation for the anhysteretic domain volume fractions requires iteration, the model takes only 20% longer than its original non-iterative version because of the small size of the iteration loop. Comparison of the model with sensing and actuation measurements reveals an average modeling error below 3%. A reduced version of the model, proposed by eliminating certain easy axis orientations, has a 30% lower computational time, with an average modeling error below 6%. © *2012 American Institute of Physics*. [doi:10.1063/1.3687372]

I. INTRODUCTION

Magnetostrictive Terfenol-D ($Tb_{0.7}Dy_{0.3}Fe_2$) is attractive for practical actuators due to its large magnetostriction (1600 ppm) and moderate saturation fields (200 kA/m). To aid in the design and control of Terfenol-D actuators, an efficient yet accurate constitutive law describing magnetization and magnetostriction in the material is needed. Modeling the fully coupled, nonlinear constitutive behavior of Terfenol-D has traditionally been a difficult problem. Its large magnetostriction anisotropy, low magnetocrystalline anisotropy, and a twinned dendritic structure give rise to complex domain level processes which are not completely understood.[1] The aim of this work is to describe the actuation and sensing response of Terfenol-D over a range of magnetic fields and stresses. To this end, we modify an efficient energy-averaged constitutive model originally developed for Galfenol. The primary benefits of the model for design and control applications are its accuracy and computational efficiency.

The Jiles-Atherton model[2] was originally formulated for isotropic ferromagnetic hysteresis. The total magnetization of a ferromagnetic material with Weiss-type moment interactions is obtained as the sum of an irreversible component due to domain wall motion and a reversible component due to domain wall bowing. With careful understanding of the difference between local and global anhysteretic responses, the model is straightforward to implement and computationally efficient, as it involves only five parameters which can be directly correlated to measurements. For this reason, the Jiles-Atherton model has been used to describe the behavior of Terfenol-D actuators in which the magnetostriction is modeled as a quadratic function of magnetization.[3–5]

The Preisach model[6] generates smooth ferromagnetic hysteresis curves through contributions from a large number of elementary bistable hysterons. Because giant magnetostrictive materials such as Terfenol-D show significant deviation in behavior from elementary Preisach hysterons, Reimers and Della Torre[7,8] developed a special hysteron with a bimodally distributed susceptibility function to describe the 1D actuation response of Terfenol-D.

Carman and Mitrovic.[9] formulated a model for Terfenol-D using Gibbs free energy expanded in a Taylor series. The exact form of the series, that is the degree of truncation, and the value of the coefficients were determined experimentally. The model describes Terfenol-D actuation for low to moderate applied fields over a specific range of applied pre-stress. Zheng and Sun[10] included higher order terms in the Taylor series and used a Langevin function to describe the magnetization curve. The model, although anhysteretic, accurately describes the nonlinear nature of Terfenol-D's magnetostriction for a wide range of pre-stresses. The ΔE effect was quantified but it was only validated qualitatively.

Armstrong[11] formulated a model for Terfenol-D in which bulk magnetization and strain are obtained as an expected value of a large number of possible energy states (or moment orientations) with an energy-based probability density function. To increase the model efficiency, Armstrong[12] restricted the choice of moment orientations to the easy magnetization axes (eight <111> directions for Terfenol-D) and used a discrete version of the probability density function. The increase in computational speed, however, came at the cost of reduced accuracy due to the restricted choice of possible moment

[a)]Electronic mail: chakrabarti.3@osu.edu.
[b)]Author to whom correspondence should be addressed. Electronic mail: dapino.1@osu.edu.

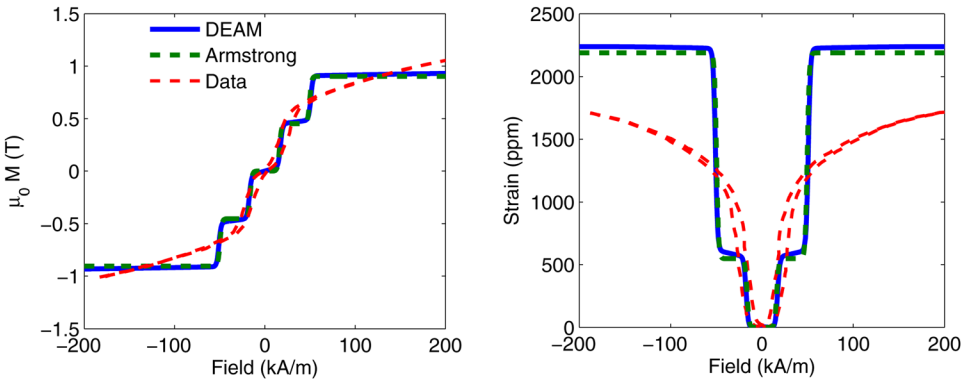

FIG. 1. (Color online) Comparison of magnetization and magnetostriction curves for Terfenol-D at 13.5 MPa compressive stress (Ref. 18) with the Armstrong model (Ref. 12) and the Discrete Energy-Averaged Model (DEAM, Ref. 14).

orientations. Atulasimha *et al.*[13] improved the accuracy of the Armstrong model by expanding the number of possible orientations to 98 crystallographic directions. Evans and Dapino[14] proposed a different approach for increasing the efficiency of the energy-averaged class of models by choosing only those orientations which minimize an energy functional locally defined around each easy axis.

The Evans and Dapino[14] Discrete Energy-Averaged Model (DEAM) has major shortcomings when applied to Terfenol-D, as detailed in Sec. II. Section III presents an anhysteretic model formulation that addresses each of those challenges; anhysteretic model results are compared with experimental data in Sec. IV. The proposed anhysteretic version of the model is fully 3D and appropriate for use in finite element modeling frameworks. An extension to model magneto-mechanical hysteresis by using an evolution equation for the domain volume fractions, similar to that of Evans and Dapino,[14] is presented in Sec. V. The hysteretic model can be used for control applications where quantification of additional delay due to material hysteresis is critical for ensuring stability. Section VI provides a quantitative description of the model's performance.

II. PROBLEM DESCRIPTION

Terfenol-D has eight minima along the <111> directions. When energy-averaged models such as the Armstrong model,[12] or the Discrete Energy-Averaged Model,[14] are compared with measurements, two major discrepancies are observed. First, these models introduce an unphysical kink in the magnetization and magnetostriction; second, the slow approach to saturation observed in the data is absent (Fig. 1). Use of a sufficiently high smoothing factor (as done by Armstrong)[12] removes the unphysical kink and somewhat smoothes out the saturation behavior. However, it results in large inaccuracies in the low to moderate field regions. Moreover, the kinking reappears at high pre-stress values (Fig. 2).

For a [112]-oriented sample, the magnetization process is governed by two distinct domain jumps: one from the $[11\bar{1}]$ and $[\bar{1}\bar{1}1]$ directions perpendicular to the sample axis to the $[1\bar{1}1]$ and $[\bar{1}11]$ directions oriented 61.9° from the sample growth axis, and the second from $[1\bar{1}1]$ and $[\bar{1}11]$ to the [111] direction oriented 19.5° from the growth axis. When no compressive prestress is applied, all the <111> orientations have equal energy and the jumps occur at very low magnetic fields. Application of compressive prestress alters the energy of each of the three sets of orientations. The energy due to applied stress increases as the angle between the domain magnetization and sample axis decreases. Thus the increase in energy is largest for the [111] direction and smallest for the $[11\bar{1}]$ and $[\bar{1}\bar{1}1]$ directions. The difference in energy between the three sets of easy axes causes domains to stick at a particular set of orientations until additional magnetic field is applied to overcome the magnetoelastic energy difference between the current and the next set of orientations. This domain attachment causes kinking in the magnetization and magnetostriction curves (Fig. 3). The magnitude of the kink increases with the amount of applied prestress. Thus a high value of smoothing factor Ω, which smoothes out the kinks for smaller prestresses, cannot eliminate the kinking when the applied prestress is increased as observed in Fig. 2. A value of Ω which is high enough to smooth out the kinks for all prestresses results in the model overestimating the burst field and underestimating the slope of the magnetostrictionfield curve in the burst region. These issues imply that fundamental changes are necessary in order to successfully apply energy-averaged models to Terfenol-D.

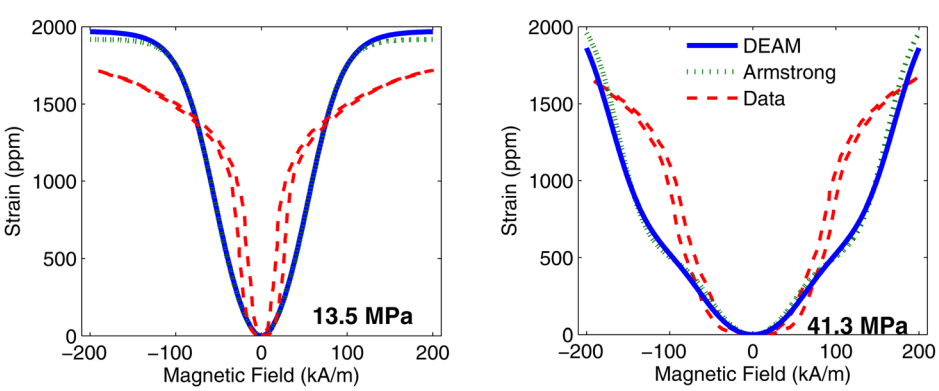

FIG. 2. (Color online) Armstrong model (Ref. 12) and DEAM (Ref. 14) with high smoothing factors for 13.5 and 41.3 MPa prestress. The higher prestress curve shows the reappearance of kinks in both models.

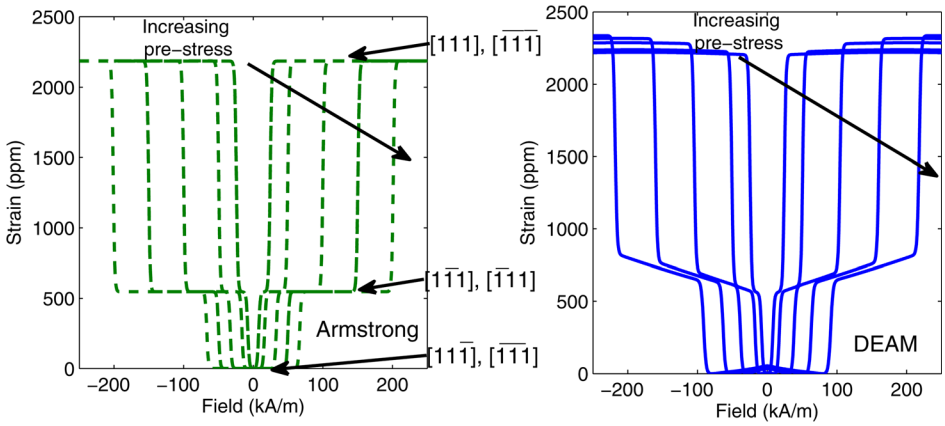

FIG. 3. (Color online) Armstrong model (Ref. 12) and DEAM (Ref. 14) with low smoothing factors showing the magnitude of the two kinks with increasing stress.

III. MODEL FORMULATION

A. Elimination of unphysical kinks

Assuming a [112]-oriented sample, the intermediate kinks occur when domains align along the [1$\bar{1}$1] and [$\bar{1}$11] directions for positive applied fields and [1$\bar{1}\bar{1}$] and [$\bar{1}$1$\bar{1}$] directions for negative applied fields. Absence of kinks in the measurements suggests that domains are prevented from orienting along these directions. This can be modeled by increasing the magnetocrystalline anisotropy energy along these orientations compared to the other easy axis orientations. In the original DEAM formulation, the anisotropy energy is defined locally around each easy axis,

$$G_A^k = \frac{1}{2}K^k\left\|\mathbf{m^k} - \mathbf{c^k}\right\|^2, \tag{1}$$

where the anisotropy constant K^k controls how steep the anisotropy energy wells are around the kth easy axis $\mathbf{c}^{\boldsymbol{k}}$. Because the anisotropy energy along each easy axis direction is identically zero, achieving variations in the base anisotropy energy between the different easy axes is not possible from Eq. (1). To achieve such variation, an orientation-dependent global anisotropy energy is superimposed onto the local anisotropy energy defined around each easy axis direction,

$$G_A^k = w^k G_{A_0}^k + \frac{1}{2}K^k\left\|\mathbf{m^k} - \mathbf{c^k}\right\|^2. \tag{2}$$

Here, $G_{A_0}^k$ is the global anisotropy energy, which for materials with cubic anisotropy is given by,

$$G_{A_0}^k = K_4\left(m_1^{k^2}m_2^{k^2} + m_2^{k^2}m_3^{k^2} + m_3^{k^2}m_1^{k^2}\right) + K_6\left(m_1^{k^2}m_2^{k^2}m_3^{k^2}\right), \tag{3}$$

In Eq. (2), $G_{A_0}^k$ is weighted by w^k, an empirical weighting factor that adjusts the anisotropy energy along the kth easy axis. Physically, the weighting accounts for the change in energy landscape that may occur due to precipitates, dislocations, and twin boundaries.[15] The eight easy axes can be broken down into three groups depending upon their angle relative to the sample axis: the [111] and [$\bar{1}\bar{1}\bar{1}$] directions oriented 19.5° with the sample axis, the [11$\bar{1}$] and [$\bar{1}$ $\bar{1}$1] directions oriented perpendicular to the sample axis, and the [1$\bar{1}$1], [$\bar{1}$11], [1$\bar{1}\bar{1}$], and [$\bar{1}$1$\bar{1}$] directions oriented 61.9° from the sample axis. Thus, there are effectively three weights that must be determined, one for each group.

Another way to suppress the kinks is to ignore the minima associated with the four orientations which cause kinking. The global anisotropy energy is still weighted but there are only two weights to be determined because the set of directions 61.9° from the sample axis is not considered. This way the number of minima is reduced to four. The first approach is more accurate as it has more degrees of freedom while the second approach is more efficient as it involves averaging of only four terms. However, in the second approach, the three-dimensional accuracy of the model is expected to suffer due to the loss of four orientations. In this paper the full version of the model is described in detail and its performance is compared to the reduced version in terms of accuracy and efficiency.

B. Obtaining the slow approach to saturation

The exact reason for the slow approach to saturation in Terfenol-D is not clearly understood. Various explanations have been proposed such as the presence of demagnetization fields,[16] or radically different behavior of twins,[17] but experimental proof is lacking. Domain observations reported by Engdahl[18] suggest that closure domains become increasingly difficult to remove in Terfenol-D as the sample is magnetized. From these theories and observations it can be postulated that with increasing applied field, there is a tendency of domains to occupy orientations which do not minimize the theoretical energy obtained by summing up the anisotropic, magnetoelastic, and Zeeman components. Incorporation of demagnetization fields in the model comes at the expense of an implicit definition for the total energy, which means that iterations need to be performed to converge to the correct value of volume fractions. Every iteration will involve computation of the energies, minima, domain volume fractions, and the bulk magnetization, adding significant computational effort to the model.

An alternative way of incorporating this apparent broadening of domain distribution is to employ a variable smoothing factor which increases as the domain volume fractions increasingly move farther away from a homogeneous distribution. Mathematically this can be written as,

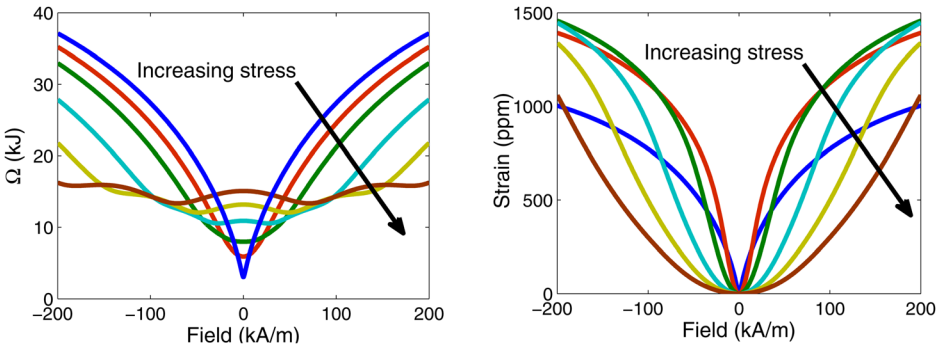

(a) (b)

FIG. 4. (Color online) (a) Ω-field and (b) strain-field curves for compressive prestresses of 0, 6.5, 13.5, 27.4, 41.3, and 55.3 MPa.

$$\Omega = a_0 + a_1 \left\| \boldsymbol{\xi}_{an}(\mathbf{H},\mathbf{T}) - \bar{\xi} \right\|^2, \tag{4}$$

where $\boldsymbol{\xi}_{an}(\mathbf{H},\mathbf{T})$ is the vector of anhysteretic domain volume fractions and $\bar{\xi}$ is a vector equal in length to $\boldsymbol{\xi}_{an}$ but with each component as $1/r$, r being the number of easy axis orientations. Both $\boldsymbol{\xi}_{an}$ and $\bar{\xi}$ are r-dimensional vectors, with $r = 8$ for Terfenol-D. When no bias stress or field is applied, assuming cubic magnetocrystalline anisotropy energy distribution, all 8 orientations are equally likely to be occupied by the domains. Thus $\xi_{an} = \bar{\xi}$ and $\Omega = a_0$, its lowest value. On application of stress or field the volume fractions will deviate away from this homogeneous distribution, causing Ω to increase. When a bias stress or field is applied, the initial domain distribution is not homogeneous, so for application of field and stress about the bias points Ω no longer increases monotonically. Figure 4(a) shows the variation of Ω with applied field for different bias stress values. At low fields the value of Ω increases with increasing bias stress while at high fields Ω is larger for a lower bias stress. This allows the magnetostriction curves for low bias stress to exhibit a sharp burst region at low fields and a gradual approach to saturation at high fields, while for the high bias stress curves the slope in the burst region is more gradual because Ω is relatively large in the burst region (Fig. 4(b)). Figure 5 shows the Ω-stress curves and the corresponding magnetization-stress curves for different bias fields. For low bias fields, Ω is small at low stresses and larger at higher stress values while for high bias fields, Ω is large for low stresses and relatively small for higher stress values. Figures 4 and 5 show the behavior of a material with perfect cubic anisotropy, in which the global anisotropy energy along all the easy axis orientations is equally weighted (i.e, w^k is the same for all k). When this is not the case, the Ω vs. field and Ω vs. stress curves will be different. At zero applied stress and field, for example, the domains will not be homogeneously distributed among the eight directions. Rather, they will be concentrated in orientations along which the weights of the global anisotropy energy are maximum.

C. Computational aspects

The new definition for Ω, expression (4), destroys the explicit nature of the model because Ω is defined as a function of $\boldsymbol{\xi}_{an}$ while determination of $\boldsymbol{\xi}_{an}$ requires knowledge of Ω according to the relation,

$$\xi_{an}^k = \frac{\exp\left(-G^k/\Omega(\boldsymbol{\xi}_{an})\right)}{\sum_{j=1}^{r} \exp\left(-G^j/\Omega(\boldsymbol{\xi}_{an})\right)}, \tag{5}$$

where ξ_{an}^k is the volume fraction of the kth easy axis. The advantage of this implicit definition over an implicit definition for energy (as in the case of demagnetization fields) is that the two most computationally intensive processes—computation of energies and the corresponding energy minima—are excluded from the iteration loop. The steps within the iteration loop include determination of the volume fractions, a convergence check, and computation of two scalar expressions for $df/d\Omega$ and Ω. These steps are fast and allow for efficient computation of the model.

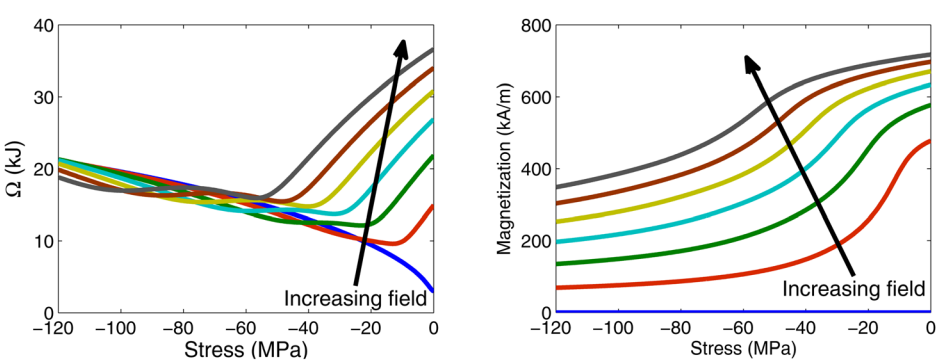

(a) (b)

FIG. 5. (Color online) (a) Ω-stress and (b) magnetization-stress curves for constant bias fields of 0, 32.2, 64.4, 96.6, 128.8, 161, and 193.2 kA/m.

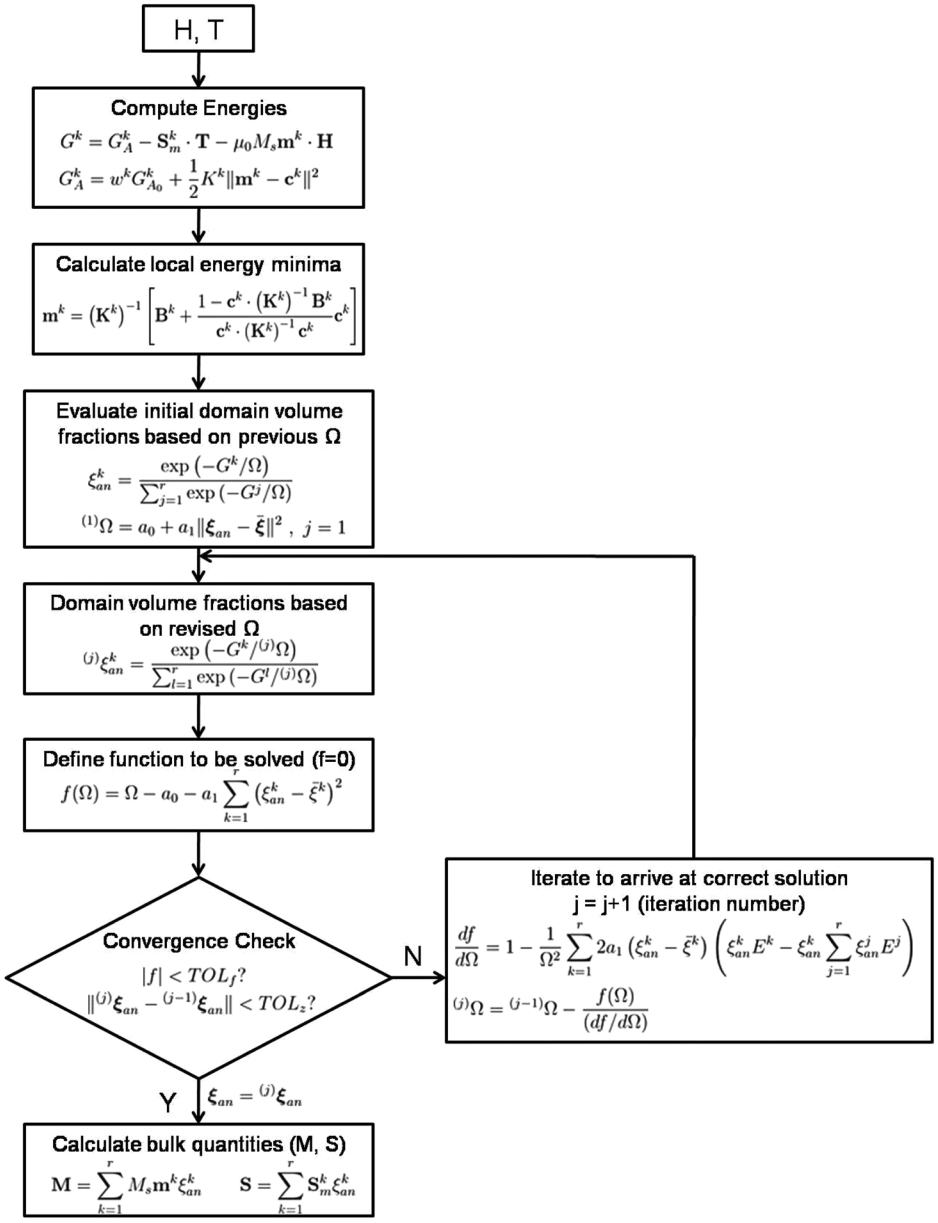

FIG. 6. Flow chart for the anhysteretic model. Details of the energy minimization can be obtained from Evans and Dapino. (Ref. 14).

The algorithm for computing the model is shown in Fig. 6. The solution loop involves combining Eqs. (4) and (5) to obtain a single equation in terms of Ω,

$$f(\Omega) = \Omega - a_0 - a_1 \sum_{k=1}^{r} \left(\xi_{an}^k - \bar{\xi}^k \right)^2 = 0. \tag{6}$$

Newton-Raphson iterations are performed for quick convergence because the derivative $df/d\Omega$ can be analytically obtained as,

$$\frac{df}{d\Omega} = 1 - \frac{1}{\Omega^2} \sum_{k=1}^{r} 2a_1 \left(\xi_{an}^k - \bar{\xi}^k \right) \left(\xi_{an}^k G^k - \xi_{an}^k \sum_{j=1}^{r} \xi_{an}^j G^j \right). \tag{7}$$

Even with strict tolerances, usually two to three iterations are sufficient for convergence.

To investigate the effect of this iterative procedure on the model efficiency, the model is run with and without iterations for a large number of inputs. It is found that on average the iterative version takes only 20% longer than the non-iterative one.

IV. ANHYSTERETIC MODEL RESULTS

The model is compared with actuation measurements from Moffett *et al.*[19] and sensing measurements from Kellogg and Flatau.[20] Anhysteretic model parameters have been obtained by extracting the anhysteretic curves from data (using simple averaging of values from the upper and lower branches of the major hysteresis loops[21]) and using a least squares optimization algorithm. The full model with eight minima contains nine parameters (K, M_s, λ_{100}, λ_{111}, a_0, a_1, $w^1 = w^2$, $w^3 = w^4$, $w^5 = w^6 = w^7 = w^8$) while the model with four minima contains eight parameters due to the absence of w^5 through w^8.

Figure 7 shows the performance of the two models when optimized to describe the magnetostriction measurements of

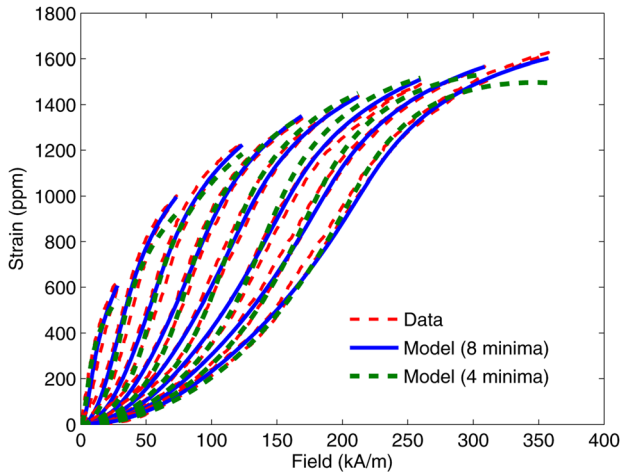

FIG. 7. (Color online) Comparison of the full model (eight minima), reduced model (four minima), and actuation data (Ref. 19) for compressive prestresses of 6.9, 15.3, 23.6, 32.0, 40.4, 48.7, 57.1, and 65.4 MPa.

Moffett *et al.*[19] Both models can accurately describe the measurements. However, the reduced version shows some error near saturation, particularly for the high bias stress curves. With parameters optimized for the strain-field curves, the full model accurately describes the stress-strain response (Fig. 8).

To apply the model to various material compositions and operating conditions, the parameters were also optimized for Terfenol-D sensing measurements reported by Kellogg and Flatau.[20] Throughout the paper an elastic modulus of 115 GPa is used, calculated using the slope of the strain-stress curves at high compressive stresses and low bias fields. Figure 9 reveals that the full version of the model is able to describe the trends more accurately than the reduced version with four minima.

V. EXTENSION TO HYSTERETIC MODEL

The model can be extended to include hysteresis with an incremental formulation similar to that done by Evans and Dapino.[14] The total volume fraction increment can be written as a combination of an anhysteretic and an irreversible component,

$$d\xi^k = c d\xi^k_{an} + (1-c) d\xi^k_{irr}, \tag{8}$$

where $d\,\xi^k_{irr}$ is given by

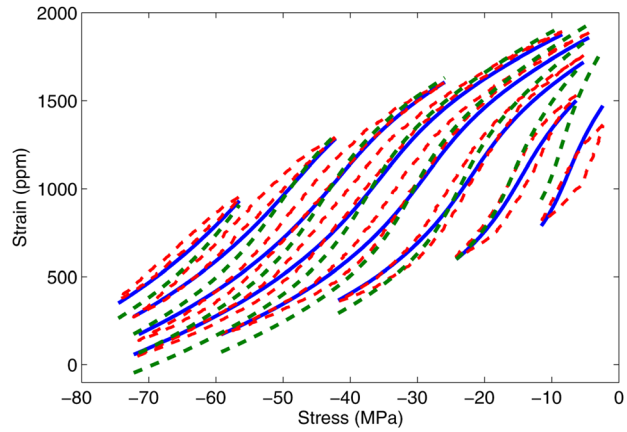

FIG. 8. (Color online) Performance of the full and reduced models in predicting the stress-strain behavior of Terfenol-D (Ref. 19) for bias field values of 11.9, 31.8, 55.7, 79.3, 103, 127, 151, and 175 kA/m with parameters estimated from the strain-field curves.

$$\begin{aligned} d\xi^k_{irr} = \frac{\zeta}{k_p}(\xi^k_{an} - \xi^k_{irr})[\mu_0 M_s(|dH_1| + |dH_2| + |dH_3|) \\ + (3/2)\lambda_{100}(|dT_1| + |dT_2| + |dT_3|) \\ + 3\lambda_{111}(|dT_4| + |dT_5| + |dT_6|)], \end{aligned} \tag{9}$$

and $d\xi^k_{an}$ is given by

$$d\xi^k_{an} = \frac{\partial \xi^k_{an}}{\partial \mathbf{H}} d\mathbf{H} + \frac{\partial \xi^k_{an}}{\partial \mathbf{T}} d\mathbf{T}. \tag{10}$$

The calculation of partial derivatives $\partial\xi^k_{an}/\partial\mathbf{H}$ and $\partial\xi^k_{an}/\partial\mathbf{T}$ for the traditional energy-averaged model is much simpler because ξ^k_{an} is explicitly defined in terms of **H** and **T.** Although ξ^k_{an} is implicit as given by Eq. (5) it is possible to obtain an analytical expression for its derivatives,

$$\begin{aligned} \frac{\partial \xi^k_{an}}{\partial H_i} = \alpha^k - \xi^k_{an}\sum_{j=1}^{r}\alpha^j + 2a_1(\boldsymbol{\xi_{an}} - \bar{\boldsymbol{\xi}}) \\ \cdot \left(\frac{d\boldsymbol{\xi_{an}}}{dH_i}\right)\left(\beta^k - \xi^k_{an}\sum_{j=1}^{r}\beta^j\right), \end{aligned} \tag{11}$$

where,

$$\alpha^k = -\frac{\xi^k_{an}}{a}\left(\frac{\partial G^k}{\partial H_i}\right), \tag{12}$$

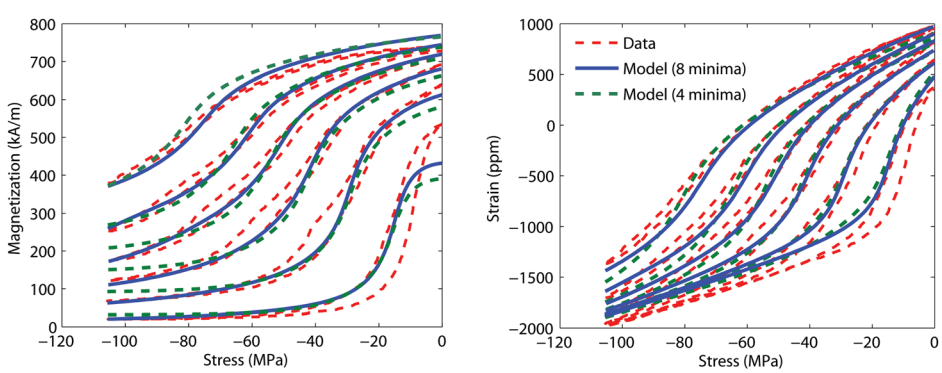

FIG. 9. (Color online) Comparison of the full model, reduced model, and sensing data from Ref. 20 for bias magnetic fields of 16.1, 48.3, 80.5, 112.7, 144.9, and 193.2 kA/m.

TABLE I. Mean percent errors obtained with the full and reduced models (Maximum percent errors in parentheses).

Data	Eight minima	Four minima
Moffett *et al.*[19] (strain-field)	1.1 (3.4)	2.3 (11.2)
Moffett *et al.*[19] (strain-stress with parameters optimized for strain-field loops)	2.3 (6.3)	5.7 (20.3)
Etrema Products, Inc.[23]	1.2 (5.2)	2.5 (10.3)
Kellogg and Flatau[20]	1.6 (9.87)	1.97 (12.8)
Simulation time (for Moffett *et al.*[19] data)	0.206 s	0.146 s

$$\beta^k = \frac{\xi_{an}^k}{a^2} G^k, \tag{13}$$

$$(\boldsymbol{\xi_{an}} - \bar{\boldsymbol{\xi}}) \cdot \left(\frac{d\boldsymbol{\xi_{an}}}{dH_i}\right) = \frac{\sum_{k=1}^{r}\left(\alpha^k - \xi_{an}^k \sum_{j=1}^{r} \alpha^j\right)\left(\xi_{an}^k - \bar{\xi}^k\right)}{1 - 2a_1 \sum_{k=1}^{r}\left(\beta^k - \xi_{an}^k \sum_{j=1}^{r} \beta^j\right)\left(\xi_{an}^k - \bar{\xi}^k\right)}. \tag{14}$$

The derivative $\partial G^k/\partial H_i$ can be obtained as done by Chakrabarti and Dapino.[22] Equation (14) is obtained by multiplying Eq. (11) by $(\xi_{an}^k - \bar{\xi}^k)$ and summing for all k. The partial derivatives with respect to T_i can be computed following a similar procedure.

VI. HYSTERETIC MODEL RESULTS

The performance of the hysteretic model is described quantitatively in this section by comparing it with the same data sets. Additionally, the parameters have been optimized to describe Terfenol-D magnetostriction data supplied by Etrema Products, Inc.[23] As done previously, every data set is simulated with a single set of parameters. However, the parameters are allowed to vary from one set to another because they represent measurements on samples with different compositions. The parameter optimization for the hysteretic model is done using the same least square optimization algorithm as described earlier. The hysteretic model contains two additional parameters (c and k_p) over the anhysteretic version, thus making the total number of parameters 11 and 10 for the full and reduced models, respectively. However, the optimization routine is not time consuming because the parameter values are very close to what they were for the anhysteretic version. The range for the additional parameters is also straightforward to estimate as k_p determines the width of the hysteresis loops, which is estimated to lie between 4–10 kJ while c is the reversibility coefficient, the value of which is usually between 0.05 and 0.15.

For every curve, the modeling error has been quantified using a normalized RMS error definition. The error for the ith curve in a data set is given as,

$$error = \frac{1}{range(\mathbf{X})}\sqrt{\frac{\sum_{j=1}^{N_i}\left(Y_{ij} - X_{ij}\right)^2}{N_i}}, \tag{15}$$

where Y_{ij} and X_{ij} are the jth component of the ith model vector and data vector, respectively, each containing N_i points, and $range(\mathbf{X})$ is the difference between the upper and lower bound for the entire set. A mean error for the entire data set is obtained by averaging the normalized RMS error for all curves in the set. A maximum error is computed by finding the maximum of the error values for all points for all curves in the data set. This gives a measure of the worst case performance of the model. Table I summarizes the mean and the maximum errors obtained for three different data sets.

For clarity, in this section only plots for the full version of the model are shown. Figure 10 shows the performance of the hysteretic model in describing the measurements reported by Moffett *et al.*[19] As before, the parameters are optimized only for the magnetostriction curves. As shown in Table I, excellent accuracy is achieved not only for the magnetostriction curves (1.1% mean error) but also for the stress-strain curves (2.3% mean error) even though no separate parameter optimization was done. The reduced model also provides high overall accuracy except for high fields and stresses. As observed for the anhysteretic version of the reduced model, some errors were found in the stress-strain response, particularly in the low stress, low field region where the maximum error is about 20%.

Similar results are obtained for sensing measurements reported by Kellogg and Flatau[20] for $Tb_{0.3}Dy_{0.7}Fe_2$. In this case the parameters are optimized for both magnetization-stress and strain-stress curves together and mean errors

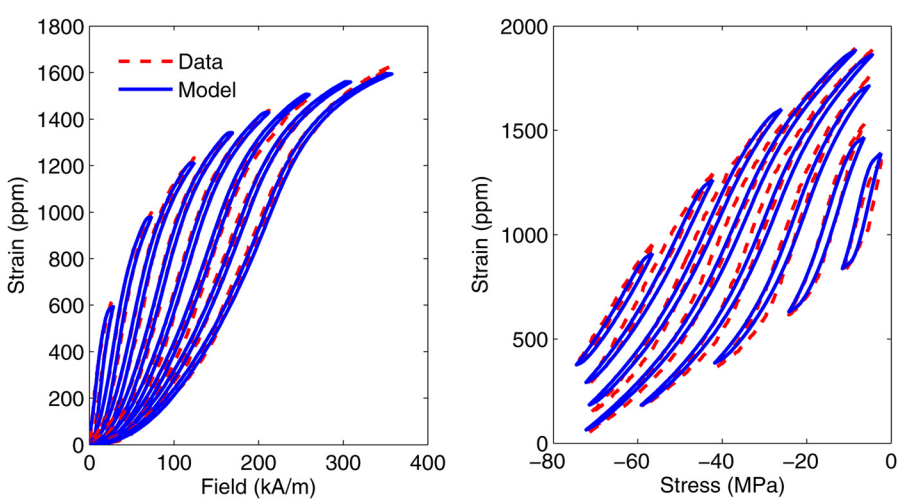

FIG. 10. (Color online) Comparison of hysteretic model with data from Moffett *et al.* (Ref. 19) for compressive prestresses of 6.9, 15.3, 23.6, 32.0, 40.4, 48.7, 57.1, and 65.4 MPa. Parameters optimized for actuation curves.

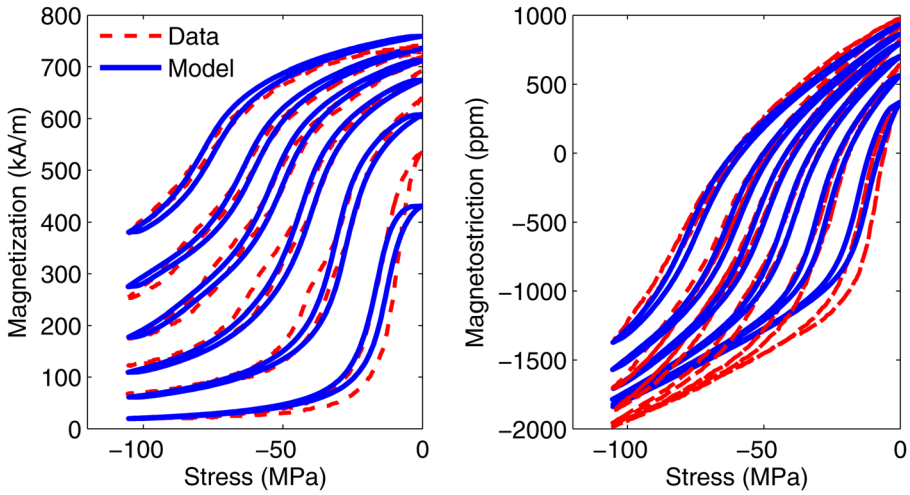

FIG. 11. (Color online) Comparison of hysteretic model with sensing data from Kellogg and Flatau (Ref. 20) for bias magnetic fields of 16.1, 48.3, 80.5, 112.7, 144.9, and 193.2 kA/m.

below 2% are obtained. The maximum error is relatively large in both versions of the model due to the discrepancy in the initial (0 stress) magnetization description of the 16.1 kA/m bias field curve.

Finally, the parameters are optimized to describe the magnetostriction curves for commercially available Terfenol-D supplied by Etrema Products, Inc.[23] (See Fig. 12.) The model accurately describes both saturation nonlinearity and hysteresis. For example, at high compressive prestresses, the magnetization process is dominated by reversible domain rotation giving rise to a nearly anhysteretic response. This is seen both in the experimental and modeled magnetostriction curves at 16 ksi (110.4 MPa). The model also describes the effect of preload on the maximum magnetostriction. For example, the 1 ksi (6.9 MPa) curve exhibits a lower saturation magnetostriction than the 4 ksi (27.6 MPa) and 8 ksi (55.2 MPa) curves. The optimized parameters for every data set for both versions of the model are shown in Table II. To compare the efficiencies of the two models, the time taken by each to simulate the Moffett *et al.*[19] data set is clocked in MATLAB. The reduced model takes about 30% less time than the full version. Thus, the reduced version can be used in applications where some accuracy can be sacrificed in the interest of computational speed.

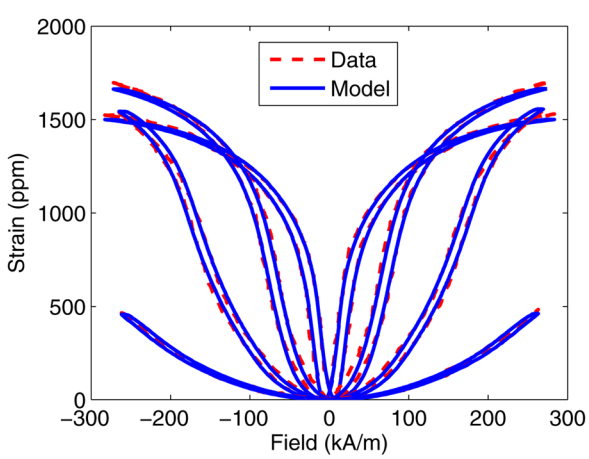

FIG. 12. (Color online) Comparison of hysteretic model with magnetostriction measurements provided by Etrema Products, Inc. (Ref. 23), for compressive prestresses of 1, 4, 8, and 16 ksi (6.9, 27.6, 55.2, 110.4 MPa).

VII. CONCLUDING REMARKS

The paper presents a fully coupled energy-averaged constitutive model to describe the magnetomechanical response of Terfenol-D. Two main deficiencies of previous energy-averaged models for Terfenol-D are recognized and addressed. One is the presence of an unphysical kink in the modeled response, which is absent in measurements, and the other is the absence of the slow approach to saturation present in Terfenol-D magnetostriction. It is shown that by using a weighted global anisotropy energy combined with a variable smoothing factor based on the deviation of domain volume fractions from a homogeneous distribution one is able to address both issues. The anhysteretic model is fully 3D and is appropriate for use in distributed parameter modeling frameworks. The addition of an implicit relationship for the domain volume fractions creates the need for equilibrium iterations to achieve convergence. Nevertheless, the iteration procedure is extremely efficient and is shown to take only 20% longer time than without iterations. A reduced version of the model is also proposed by ignoring the four minima corresponding to the four easy axes orientations which cause the kinks. This approach is more efficient but suffers from some loss of accuracy under specific conditions of high stress and field for actuation and low stress and field for sensing.

A hysteretic extension to the model is formulated based on an evolution equation for the domain volume fractions. This model is used to simulate the response of three different data sets. The model accurately describes the regions with and without hysteresis and achieves below 3% mean error for all the sets. The reduced version exhibits slightly lower accuracy but requires 30% less computer time than the full version. The hysteretic model is useful for implementation in control design where quantifying delays due to hysteresis is of importance.

ACKNOWLEDGMENTS

The authors wish to acknowledge the financial support by the member organizations of the Smart Vehicle Concepts Center (www.SmartVehicleCenter.org), a National Science Foundation Industry/University Cooperative Research

TABLE II. Optimized model parameters for the different data sets.

	Moffett *et al*. (Ref. 19)		Kellogg and Flatau (Ref. 20)		Etrema Products, Inc. (Ref. 23)	
Parameters	Eight minima	Four minima	Eight minima	Four minima	Eight minima	Four minima
$K \times 10^5$ (J/m^3)	4.306	2.409	17.68	3.049	4.602	2.188
$\mu_0 M_s$ (T)	1.025	0.892	1.047	0.975	0.964	0.891
$\lambda_{100} \times 10^3$	0.114	0.126	0.093	0.114	0.104	0.094
$\lambda_{111} \times 10^3$	1.546	1.554	1.486	1.348	1.424	1.428
$a_0 \times 10^3$ (J)	1.776	0.600	4.611	7.202	1.93	0.6
$a_1 \times 10^3$ (J)	92.49	150.4	44.69	50.7	43.11	70.77
$w^{(1,2)}$	1.119	1.149	1.341	1.252	1.068	1.062
$w^{(3,4)}$	0.940	0.846	0.844	0.748	1.056	1.061
$w^{(5,6,7,8)}$	0.915	–	0.575	–	0.87319	–
$k_p \times 10^3$ (J)	5.582	4.215	8.376	7.802	10	9.297
c	0.15	0.15	0.100	0.104	0.05	0.05
E_s (GPa)	115	115	115	115	115	115

Center, and by the Office of Naval Research (ONR) through MURI grant #N000140610530. Partial support for S.C. was provided by the Smart Vehicle Concepts Center Graduate Fellowship Program.

[1]Y. Huang and Y. Jin, Appl. Phys. Lett. **93**, 142504 (2008).
[2]D. Jiles and D. Atherton, J. Magn. Magn. Mater. **61**, 48 (1986).
[3]F. Calkins, R. Smith, and A. Flatau, IEEE Trans. Magn. **36**, 429 (2000).
[4]W. Huang, B. Wang, S. Cao, Y. Sun, L. Weng, and H. Chen, IEEE Trans. Magn. **43**, 1381 (2007).
[5]S. Chakrabarti and M. Dapino, Smart Mater. Struct. **19**, 055009 (2010).
[6]F. Preisach, Z. Phys. **94**, 277 (1935).
[7]A. Reimers and E. D. Torre, IEEE Trans. Magn. **35**, 1239 (1999).
[8]A. Reimers and E. D. Torre, J. Appl. Phys. **85**, 4497 (1999).
[9]G. Carman and M. Mitrovic, J. Intell. Mater. Syst. Struct. **6**, 673 (1995).
[10]X. Zheng and L. Sun, J. Appl. Phys. **100**, 063906 (2006).
[11]W. Armstrong, J. Appl. Phys. **81**, 2321 (1997).
[12]W. D. Armstrong, J. Magn. Magn. Mater. **263**, 208 (2003).
[13]J. Atulasimha, G. Akhras and A.B. Flatau, J. Appl. Phys. **103**, 07B336 (2008).
[14]P. G. Evans and M. J. Dapino, J. Appl. Phys. **107**, 063906 (2010).
[15]M. Al-Jiboory, D. Lord, Y. Bi, J. Abell, A. Hwang, and J. Teter, J. Appl. Phys. **73**, 6168 (1993).
[16]X. Zhao and D. Lord, J. Magn. Magn. Mater. **195**, 699 (1999).
[17]A. Clark, J. Teter, and O. McMasters, J. Appl. Phys. **63**, 3910 (1988).
[18]G. Engdahl, *Handbook of Giant Magnetostrictive Materials*, 1st ed. (Academic Press, New York, 2000).
[19]M. Moffett, A. Clark, M. Wun-Fogle, J. Linberg, J. Teter, and E. McLaughlin, J. Acoust. Soc. Am. **89**, 1448 (1991).
[20]R. Kellogg and A. Flatau, J. Intell. Mater. Syst. Struct. **19**, 583 (2008).
[21]M. Benbouzid, G. Reyne, G. Meunier, L. Kvarnsjo, and G. Engdahl, IEEE Trans. Magn. **31**, 1821 (1995).
[22]S. Chakrabarti and M. Dapino, Smart Materials and Structures **20**, 105034 (2011).
[23]Etrema, Inc., *Terfenol-D data sheet*, Etrema Inc., Ames, IA. See http://www.etrema-usa.com/.